#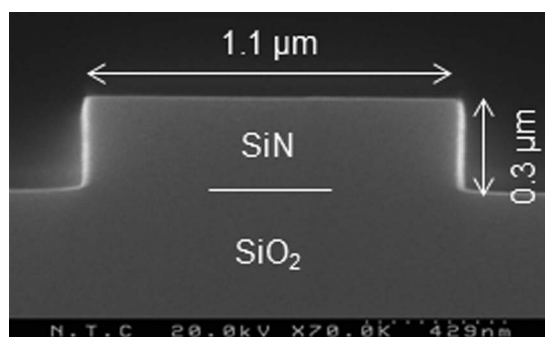 Using a Si$_3$N$_4$ Ring Resonator Notch Filter for Optical Carrier Reduction and Modulation Depth Enhancement in Radio-Over-Fiber Links

A. Perentos
F. Cuesta-Soto
A. Canciamilla
B. Vidal
L. Pierno
N. S. Losilla
F. Lopez-Royo
A. Melloni
S. Iezekiel

Using a Si$_3$N$_4$ Ring Resonator Notch Filter for Optical Carrier Reduction and Modulation Depth Enhancement in Radio-Over-Fiber Links

A. Perentos,[1] **F. Cuesta-Soto,**[2] **A. Canciamilla,**[3] **B. Vidal,**[4] **L. Pierno,**[5]
N. S. Losilla,[4] **F. Lopez-Royo,**[4] **A. Melloni,**[3] **and S. Iezekiel**[1]

[1]Department of Electrical and Computer Engineering, University of Cyprus, Nicosia 1678, Cyprus
[2]DAS Photonics, Ciudad Politécnica de la Innovación, 46022 Valencia, Spain
[3]Dipartimento di Elettronica e Informazione, Politecnico di Milano, 20133 Milan, Italy
[4]Nanophotonics Technology Center, Universidad Politécnica de Valencia, 46022 Valencia, Spain
[5]SELEX Sistemi Integrati S.p.A., 00131 Rome, Italy

Abstract: Optical carrier reduction via the use of a Si$_3$N$_4$ ring resonator notch filter (RRNF) is proposed and experimentally demonstrated as a means for improving the modulation efficiency in 10-GHz radio-over-fiber (RoF) links. The realized filter is characterized in both the optical and microwave domains and is then exploited in an RoF test bed. Experimental results show a modulation depth improvement of up to 9 dB.

Index Terms: Optical resonators, microwave photonics, silicon nanophotonics.

1. Introduction

One of the key areas of microwave photonics is the transport of microwave and millimeter-wave signals over optical fiber. This is motivated by the large bandwidth and favorable transmission characteristics of single-mode fiber. Analog microwave fiber-optic links are typically employed in applications such as radar and antenna remoting, while radio-over-fiber (RoF) is a very attractive technology for meeting existing and anticipated high bandwidth demands in cellular communications [1]. An important aspect of an RoF link is the dynamic range of the signals, which is directly related to the modulation depth, since the fiber link efficiency increases with the modulation depth. Apart from some low-cost and relatively low-bandwidth systems based on directly modulated laser diodes, much of the body of work in RoF is based on links with external modulators, and specifically Mach–Zehnder devices. However, there is a limitation on the maximum modulating microwave signal power, since in order for an external modulator to operate in its linear region, the optical carrier has to be weakly modulated by microwave signals. On the other hand, increasing the power of the optical carrier excessively compared to the sidebands results in reduced dynamic range and can damage components such as photodiodes. Moreover, the dc photocurrent that results from detection of the optical carrier directly contributes to the shot noise at the photoreceiver. One way to
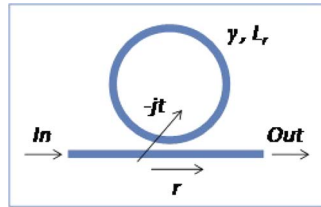
Fig. 1. RRNF structure.

mitigate these effects and to simultaneously improve link modulation efficiency is by removing a portion of the optical carrier directly after modulation. Previously reported methods for reducing the carrier include the use of Brillouin scattering [2], [3] and external optical filters such as silica delay lines [4], Fabry–Perot filters [5], fiber Bragg gratings [6], [7], and arrayed waveguide gratings (AWG) [8]. With the exception of the FBG approach, such schemes can be difficult to implement or will not operate over a wide range of modulation depths, frequencies, or formats [6]. While the FBG approach is simple to implement, it does not lend itself to monolithic integration; of the existing approaches to optical carrier reduction, only the AWG can be integrated on a photonic chip. However, AWGs are typically larger in area compared to other integrated photonics structures such as ring resonators. The application of integrated photonics to microwave photonics is an area of growing importance [9]; hence, an approach to optical carrier reduction that can align with this trend will be of interest.

Here, we propose an integrated optic filtering device for optical carrier reduction suitable for monolithic integration with a modulator and other passive and active photonic components. The proposed device has great potential for the production of low-cost and high-speed transceivers such as those required in future RoF applications, where a relatively large number of base stations are envisaged [9]. We propose and experimentally demonstrate the use of a silicon nitride (Si$_3$N$_4$) ring resonator notch filter (RRNF) to reduce the optical carrier and enhance the modulation efficiency in a 10-GHz RoF link as a proof-of-concept for application to X-band systems.

In Section 2, we outline briefly the design and fabrication of the RRNF. In Section 3, we discuss the characterization of the optical magnitude response and the RF characterization with a microwave vector network analyzer (VNA) and an optical single-sideband modulator. The development of an RoF link test bed for evaluating the suitability of the RRNF for optical carrier reduction is then described in Section 4. Experimental results indicate an improvement of up to 9 dB in the modulation depth for a 10-GHz signal.

2. Filter Design and Fabrication

The ring resonator structure shown in Fig. 1 was used to implement a notch filter. Strictly speaking, the ring resonator with a single coupler to the bus waveguide is a phase shifter, but the waveguide attenuation always induces a narrow notch at the resonance. With a careful choice of the ratio between the roundtrip attenuation and the coupling coefficient of the directional coupler, it is possible to achieve very narrow and deep notches. Although it is not the scope of this paper to discuss the theory of ring resonators, the following paragraph reports the design rules for the ring to be employed in the mentioned applications. The reader can refer to the literature for the theoretical details [10].

The ring spectral response is periodic with a free spectral range (FSR) given by FSR $=$ $c/(n_g L_r)$, where n_g is the group index of the optical waveguide, and L_r is the length of the ring. In our application, the FSR must be well above the bandwidth of the signal and should not impose severe restrictions on the bending radius of the waveguide. The coupling coefficient between the ring and the bus waveguide must be designed to provide both a narrow bandwidth and a high extinction ratio (ER), as required for carrier reduction. At resonance, the transmission vanishes when the roundtrip attenuation γ equals the field transmission coefficient $r = (1 - K)^{1/2}$ with K
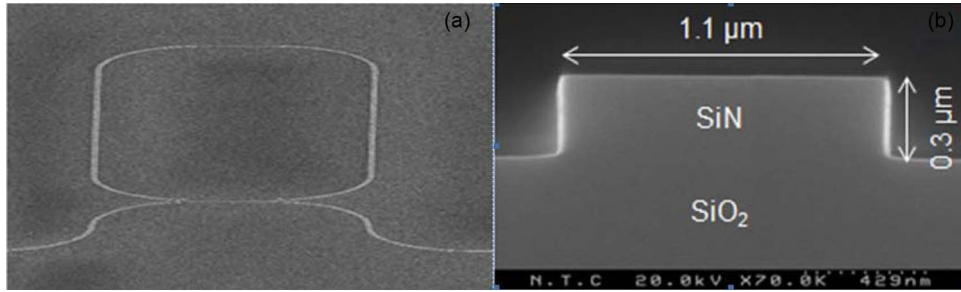
Fig. 2. SEM micrographs of the fabricated RRNF. (a) Top view of the ring and bus waveguide. (b) Cross-sectional view of the waveguide.

being the power coupling coefficient; this case is referred to as critical coupling; otherwise, the ER is defined as

$$\text{ER} = \frac{(1 + r\gamma)}{(r - \gamma)}.$$ (1)

Note that the matching of r and γ is not challenging, and a deep notch is easily obtained. Concerning the notch width (Δf), this depends on the FSR, the coupling coefficient K, and the roundtrip attenuation γ and is given by

$$\Delta f = \frac{\text{FSR}}{\pi} \sqrt{\frac{(1 - r\gamma)^2 - 2(r - \gamma)^2}{r\gamma}} \cong \frac{\text{FSR}}{\pi} \frac{K}{r}$$ (2)

with the approximation being valid when the critical coupling condition is met $(\gamma = r)$.

The RRNF has been designed with a ring radius of 100 μm, a roundtrip length of 676 μm, a coupling length of 24 μm, and a coupling coefficient K of 0.075. The coupling coefficient value was selected in order to work close to critical coupling (considering an average propagation loss of 5 dB/cm), aiming to maximize the ER and to also provide a narrow bandwidth (about 6.2 GHz) for RoF applications. The waveguide is 0.3 μm thick and 1.1 μm wide. With these choices, a good compromise between optical spectral characteristics, insertion loss, and device footprint is achieved. If the roundtrip attenuation attains the state-of-the-art values of a fraction of dB, then the notch bandwidth would be only a few hundreds of MHz. However, such a narrow bandwidth would require an accurate temperature control of the chip because in Si$_3$N$_4$, the notch shifts by roughly 1 GHz $^\circ$C^{-1}.

The device has been realized at the Nanophotonics Technology Center of the Universidad Politécnica de Valencia, Spain, using a Si$_3$N$_4$ technology platform. Si$_3$N$_4$ technology is suitable for very low loss and high yield production and has a sufficiently high index contrast to realize devices with a small footprint [11], [12]. SEM micrographs of the fabricated RRNF are shown in Fig. 2(a) and (b). The Si$_3$N$_4$ waveguide core layer was deposited using low-pressure chemical vapor deposition (LPCVD), and the structures were fabricated using standard microfabrication techniques including i-line photolithography and dry etching with a metal hard mask patterned by the liftoff technique. LPCVD is a well-known deposition technique, and Si$_3$N$_4$ deposited using this technique has generally lower optical losses than that deposited by the alternative plasma-enhanced chemical vapor deposition (PECVD).

3. RRNF Optical and Microwave-Based Characterization

3.1. Optical Characterization

The optical transmission spectrum of the RRNF was measured for TM polarization using a tunable laser source (TLS) and an optical power meter. The chip, mounted on a micropositioner,
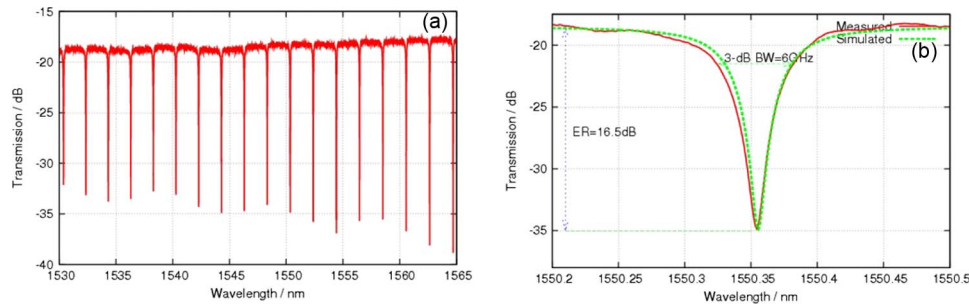
Fig. 3. Measured optical transmission spectrum of the RRNF. (a) Wavelength range 1530–1565 nm and (b) detail around resonance at 1550.35 nm overlapped with the simulated response.

was aligned in butt-coupling with lensed fibers. The measured response is shown in Fig. 3(a) over a wide wavelength range. The measured FSR is 2 nm as expected from theory. Fig. 3(b) shows the measured and simulated responses at the 1550.351-nm resonance notch. The fitting of the curves is quite accurate with an achieved ER of 16.5 dB and a 3-dB bandwidth of 6 GHz. This response is suitable for 10-GHz RoF carrier reduction.

The average fiber-to-fiber insertion loss is 18 dB, mainly due to suboptimal fiber-to-waveguide coupling. However, suitable waveguide tapers or grating couplers, as well as special small-core fibers can be used to reduce this penalty down to 1 dB per facet [11], [13]. The measured propagation losses are around 5 dB/cm. This figure is probably due to residual sidewall roughness [14] especially in the coupling sections, and efforts to finely optimize the etching process are in progress. Although the achieved attenuation is high for Si$_3$N$_4$ technology [11], [12], the impact on the spectral characteristic of the rings is limited to a slight broadening of the bandwidth, and it is not severely detrimental. A narrower and deeper notch can be achieved by reducing both the waveguide attenuation and the coupling coefficient of the directional coupler, as described in the previous section. In Fig. 3(a), the random variations of the resonant notch depth are mainly due to the waveguide backscatter [15]. This can be reduced with smoother waveguides but will be an issue only for transmission systems employing several carriers at different wavelengths.

3.2. Microwave-Based Characterization

In order to gain further insight into the notch characteristics of the RRNF, we implemented an optical VNA test bed using the techniques described in [16]. This approach is based on optical single-sideband (OSSB) modulation that employs a dual-drive Mach–Zehnder modulator (DD-MZM) and a microwave VNA to act as a swept RF input to the modulator. The test system used is shown in Fig. 4; here, the VNA is operated in forward transmission mode in order to measure the corresponding S$_{21}$ of the assembly of components connected between ports 1 and 2. The RRNF is the optical device-under-test (DUT). Owing to the use of a single sideband (as opposed to double-sideband operation as employed in lightwave component analysis [17]), this system measures the magnitude and phase response of the optical DUT as a function of the optical frequency $\omega_C + \omega_m$. Here, ω_C is the optical carrier frequency, ω_m is the microwave modulation frequency, and it is assumed that the system is calibrated at the optical DUT ports. One of the major advantages of this approach is that by using the microwave source of the VNA, finer resolution is possible over the method used in Section 3.1.

The TLS was initially set to a wavelength just before the specific resonance of the RRNF shown in Fig. 3(b). The DD-MZM was configured with the use of a 3-dB 90° hybrid to provide OSSB modulation in which the lower sideband was heavily suppressed (viz. leaving the optical carrier and upper sideband). An optical spectrum analyzer (OSA) was used in the setup to verify OSSB operation. Port 1 of the VNA was used as an RF swept generator to the RF input ports of the modulator, while port 2 was connected to a photodiode. In this setup, for a fixed optical wavelength as stated above, the VNA was swept from 500 MHz to 40 GHz with a power level of 0 dBm applied
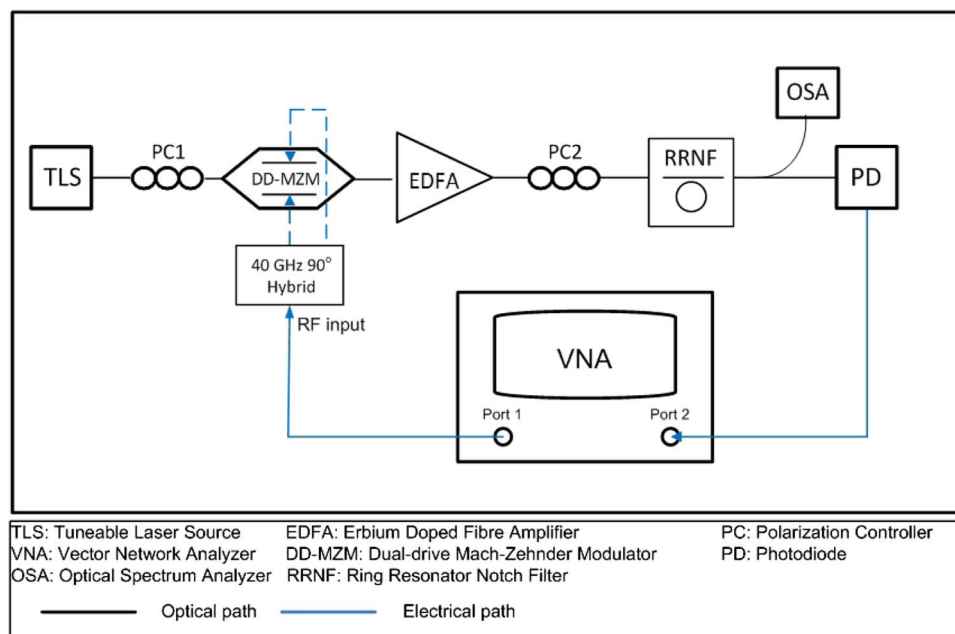
Fig. 4. Characterization test bed using OSSB modulation.

to the input of the 90° hybrid. The output signal of the DD-MZM was then amplified with an erbium-doped fiber amplifier (EDFA). The DUT (in this case, the RRNF) was then inserted into the system, and by sweeping the RF input to the modulator, it was characterized by measuring the S_{21} magnitude response with the VNA. Calibration of the test setup shown in Fig. 4 was performed by using an optical thru-connection in place of the RRNF.

Provided the optical carrier wavelength is placed sufficiently close to (and just before) the notch resonance, then as the VNA sweeps in frequency, the upper sideband is scanned across the optical transmission response of the RRNF in a region containing the notch. For a fixed optical carrier wavelength, this means that when the sideband is at the notch resonance, it is effectively filtered out, leaving only the carrier and thus resulting in negligible RF photocurrent. Thus, any resonance appearing in the magnitude response at a given fixed optical wavelength corresponds to the filtering-suppression of the upper optical sideband, thereby validating the mechanism of the notch filter. A graphical representation of this measurement approach and the effect on the actual optical spectra at each point is shown in Fig. 5.

The above measurement technique was performed at five different optical carrier wavelengths, with a separation of 0.05 nm (corresponding to a frequency separation of 6.2 GHz) between adjacent carriers. The magnitude response and unwrapped phase response are shown in Figs. 6 and 7, respectively. From Fig. 6, it is seen that for a carrier wavelength of 1550.601 nm, which falls just after the notch, the measured magnitude response does not exhibit resonance, and the upper sideband essentially sees a flat optical magnitude response. As the carrier wavelength is reduced, the microwave notch is moved toward higher microwave frequencies. A variation of 7 dB is experienced in the ER of Fig. 6 due to the extra noise added by the EDFA caused by the way the measurements were carried out. To compare the different modulation depths obtained with the ring resonator, the optical power at the input of the photodiode has to be the same (ideally, the maximum without damaging the photodiode). In the experiments, this has been done by adjusting the EDFA gain to keep the same optical power at the photodiode. The higher gain needed for the notch at low microwave frequencies (i.e., when the optical carrier is partially attenuated by the filter response) results in extra noise (and reduced filter ER). The insets of Fig. 7 show the phase change relative to the linear change around the resonances of 18.45 GHz (for $\lambda = 1550.401$ nm) and 25.5 GHz (for $\lambda = 1550.351$ nm), respectively. The phase change is approximately 150° for the
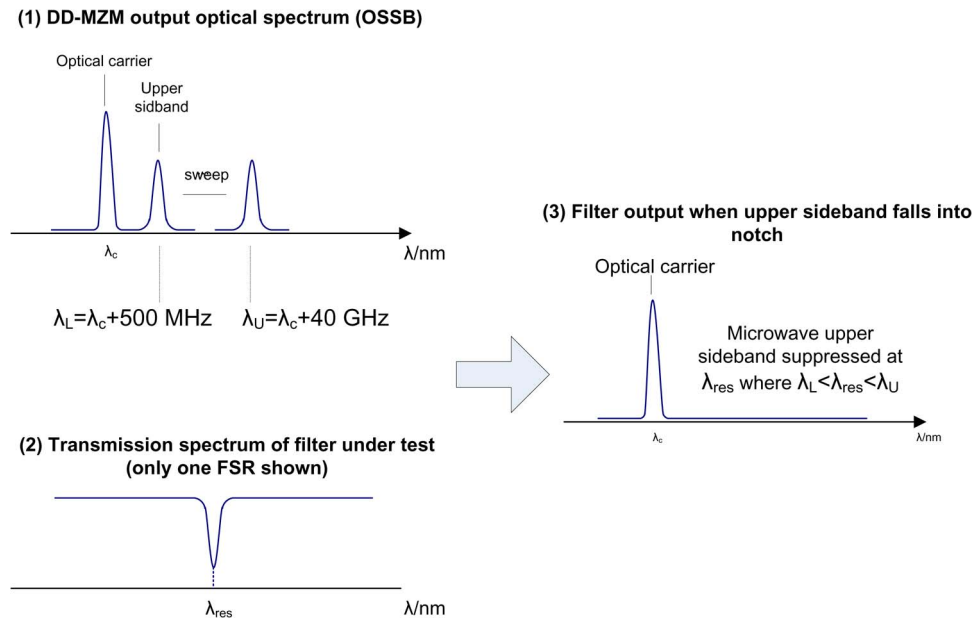
(1) DD-MZM output optical spectrum (OSSB)

Optical carrier

Upper
sidband

sweep

λ_c λ/nm

$\lambda_L = \lambda_c + 500$ MHz $\lambda_U = \lambda_c + 40$ GHz

(3) Filter output when upper sideband falls into notch

Optical carrier

Microwave upper
sideband suppressed at
λ_{res} where $\lambda_L < \lambda_{res} < \lambda_U$

λ_c λ/nm

**(2) Transmission spectrum of filter under test
(only one FSR shown)**

λ_{res} λ/nm

Fig. 5. Mechanism of upper sideband suppression. If the carrier wavelength of the OSSB signal (1) is placed just to the left of λ_{res} in the filter transmission spectrum (2), then as the sideband is swept, it will be suppressed when its wavelength reaches λ_{res} (3).

λ = 1550.351 nm
λ = 1550.401 nm
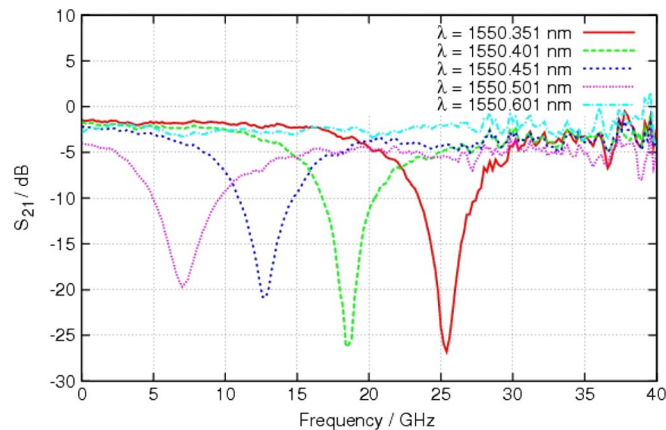λ = 1550.451 nm
λ = 1550.501 nm
λ = 1550.601 nm

Fig. 6. Measured magnitude response.

25.5-GHz resonance (from 25 GHz to 26 GHz) and 120° for the 18.45-GHz resonance (from 18 GHz to 19 GHz). A phase change to the sideband will result in a narrowband phase shift of the photo-detected signal.

4. 10-GHz Carrier-Reduced RoF Experiment for Modulation Efficiency Enhancement

The test bed shown in Fig. 8 was used to evaluate the potential for optical carrier reduction with the fabricated RRNF. The TLS, set at 7 dBm, drove an MZM biased at quadrature, and the optical carrier was modulated by a 10-GHz sinusoidal signal of 5-dBm power. This produced a double-sideband signal. An EDFA was used immediately after the MZM in order to boost the signal power entering the RRNF, while an optical bandpass filter (OBPF) was used to reduce the EDFA's
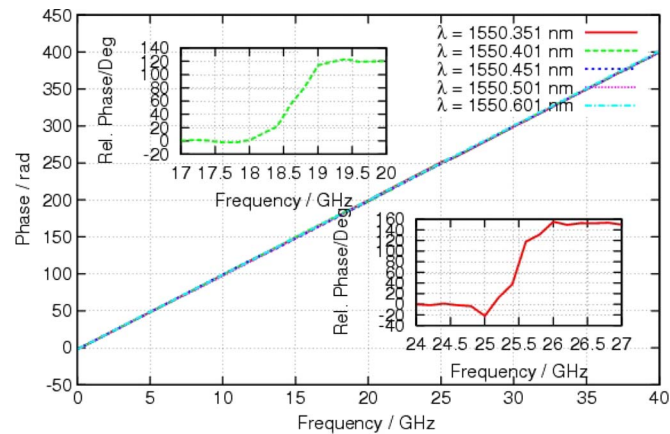
Fig. 7. Measured unwrapped phase response. The insets show the magnifications of the phase change relative to the linear change around the resonances of 18.45 GHz for $\lambda = 1550.401$ nm (top left inset) and 25.5 GHz for $\lambda = 1550.351$ nm (bottom right inset).
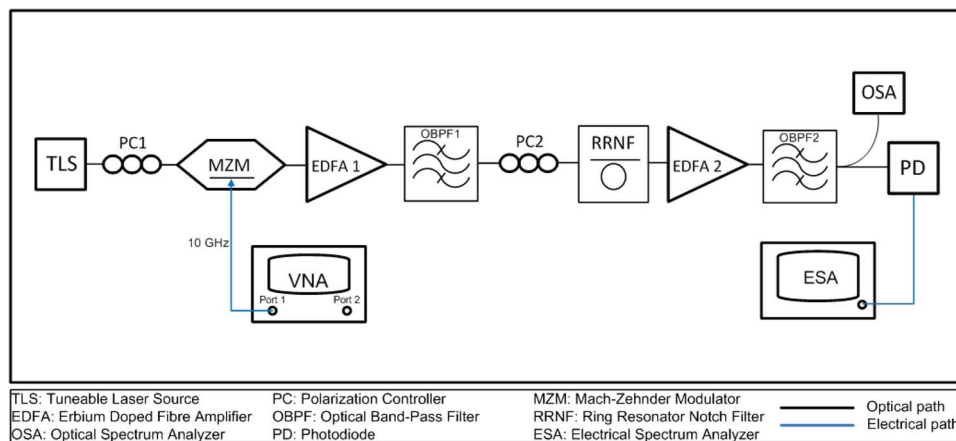

Fig. 8. RoF test bed to evaluate suitability of RRNF for carrier reduction and modulation efficiency enhancement for 10-GHz RoF.

spontaneous emission noise. The RRNF was then inserted in the system along with a polarization controller (PC) in order to select the polarization state of light coupled to the filter. The RRNF was used to reduce the carrier by the following mechanism. The optical carrier wavelength was moved into the filter notch until optimum carrier reduction was achieved. Optimum carrier reduction is achieved when the power level of the carrier aligns with the power level of the sidebands. With the optical carrier moving toward the minimum point in the filter notch, a steady improvement in the carrier-to-sideband-ratio (CSR) is observed, thus increasing the modulation depth.

In order to keep the optical power at the input of the photodiode constant with changing optical wavelength, another EDFA was used at the RRNF output along with another OBPF. The TLS was initially set to $\lambda = 1550.25$ nm, lying just before the beginning of the notch shown in Fig. 3(b), and the optical spectrum was measured with an OSA. This measurement was repeated for several slightly shifted wavelengths in order to realize a varying amount of carrier reduction and hence an improved (lower) CSR. For all wavelengths, the incident power to the OSA was kept constant at 5.3 dBm. The results are shown in Fig. 9. At $\lambda = 1550.25$ nm, the notch of the filter does not coincide with the optical carrier or upper sideband [see Fig. 9(a)] yielding a CSR of 22.44 dB. When the source wavelength shifts to 1550.34 nm [see Fig. 9(b)], the optical carrier starts to enter the slope of the filter notch, thus reducing the CSR to 21.13 dB. The best achievable CSR of 13.43 dB is obtained
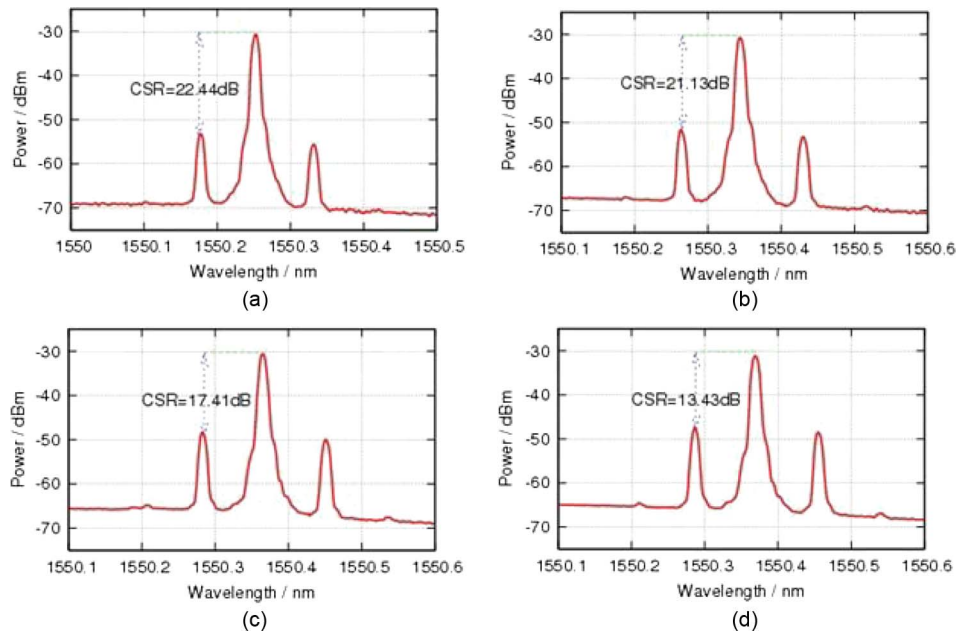
Fig. 9. Optical spectra of the carrier-reduced modulated 10 GHz for (a) no carrier reduction, $\lambda = 1550.25$ nm and CSR = 22.44 dB, (b) $\lambda = 1550.34$ nm and CSR = 21.13 dB, (c) $\lambda = 1550.36$ nm and CSR = 17.41 dB, and (d) $\lambda = 1550.37$ nm and CSR = 13.43 dB.

at $\lambda = 1550.37$ nm, and the respective spectrum is shown in Fig. 9(d). It can be observed from all plots of Fig. 9 that the lower and upper sidebands are somehow unbalanced. In fact, they appear to be uneven because the overall measured response is skewed as observed from the slope of the noise floor. This is probably attributed to the calibration of the OSA. A resonance wavelength drift (blue shift) of 0.019 nm occurs, shifting the resonance from 1550.351 nm to 1550.37 nm. This is due to the absence of a thermooptic heater and Peltier cell to finely control the resonance as well as polarization drifts associated with touching unfixed fibers in the setup and butt-coupled device. As the wavelength moves away from this value, the CSR increases again. It can be concluded from the spectra of Fig. 9 that the realized filter is suitable for the purpose of carrier reduction, achieving a CSR of 13.43 dB and a modulation depth improvement of approximately 9 dB. The modulation depth could, in theory, be improved by the ER amount of the filter shown in Fig. 3(b), i.e., by 16.5 dB (yielding a CSR of approximately 6 dB); however, this is limited to 9 dB due to the ASE noise introduced to the system by the EDFA. Measurements of the modulated optical spectra were then taken for a greater number and range of wavelengths, i.e., from 1550.25 nm to 1550.43 nm. Fig. 10 shows the corresponding variation of optical CSR, which ranges from 22.44 dB down to 13.27 dB and then rising to 25 dB.

To confirm the enhancement in modulation efficiency, the photo-converted electrical signal was measured with an electrical spectrum analyzer (ESA). The variation of the fundamental RF power with wavelength is shown in Fig. 11. For a wavelength variation from 1550.28 nm to 1550.37 nm, the RF power at 10-GHz increases from -61 dBm to -47 dBm, which is the maximum point and corresponds to the optimum CSR of 13.43 dB.

5. Conclusion

We have demonstrated the application of a Si$_3$N$_4$ RRNF for optical carrier reduction in a 10-GHz RoF link. The proposed technique allows the control of the modulation depth, which, in turn, leads to enhancement of the RoF link efficiency. A minimum CSR of 13.43 dB has been measured, with a modulation depth improvement of 9 dB. At the minimum CSR, a maximum photo-converted RF power of -47 dBm is obtained.
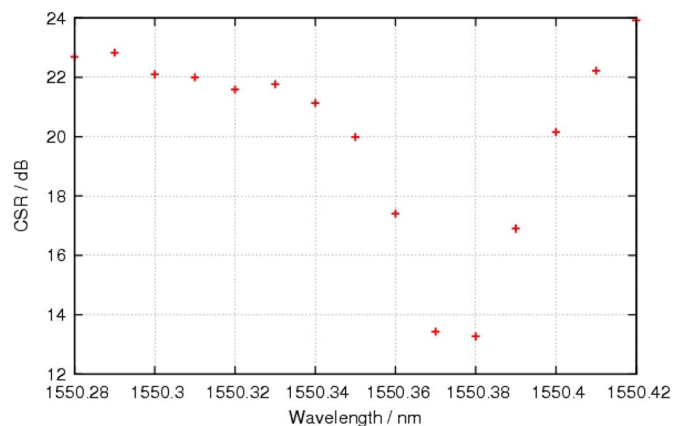
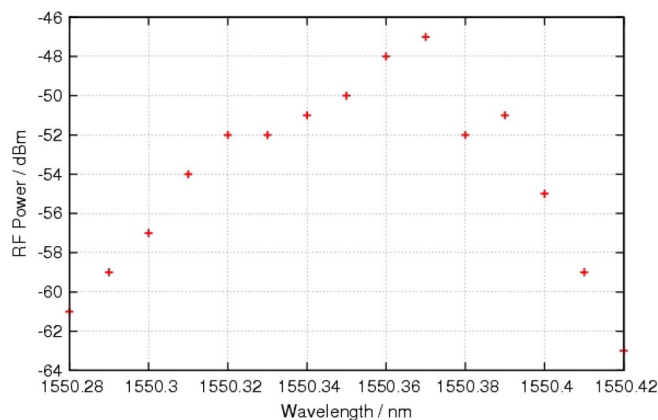Fig. 10. Measured optical CSR versus optical source wavelength.

Fig. 11. Measured fundamental RF power versus optical source wavelength.

The advantage of this method, apart from its simplicity, is that it offers the option for monolithic integration on silicon with other devices such as modulators and multiplexers as part of a photonic integrated circuit for RoF and other microwave photonic applications (such as antenna remoting and radar). Although our initial demonstrations have focused on 10 GHz, the design requirements on the RRNF would be more relaxed for higher frequencies. Hence, it is relatively straightforward to modify the design parameters for applications such as V-band and E-band RoF.

References

[1] C. Lim, A. Nirmalathas, M. Bakaul, P. Gamage, K. Lee, Y. Yang, D. Novak, and R. Waterhouse, "Fiber-wireless networks and subsystem technologies," *J. Lightw. Technol.*, vol. 28, no. 4, pp. 390–405, Feb. 2010.
[2] K. J. Williams and R. D. Esman, "Stimulated Brillouin scattering for improvement of microwave fibre-optic link efficiency," *Electron. Lett.*, vol. 30, no. 23, pp. 1965–1966, Nov. 1994.
[3] S. Tonda-Goldstein, D. Dolfi, J.-P. Huignard, G. Charlet, and J. Chazelas, "Stimulated Brillouin scattering for microwave signal modulation depth increase in optical links," *Electron. Lett.*, vol. 36, no. 11, pp. 944–946, May 2000.
[4] M. J. LaGasse, W. Charczenko, M. C. Hamilton, and S. Thaniyavarn, "Optical carrier filtering for high dynamic range fiber optic links," *Electron. Lett.*, vol. 30, no. 25, pp. 2157–2158, Dec. 1994.
[5] R. D. Esman and K. J. Williams, "Wideband efficiency improvement of fiber optic systems by carrier subtraction," *IEEE Photon. Technol. Lett.*, vol. 7, no. 2, pp. 218–220, Feb. 1995.
[6] M. Attygalle, C. Lim, G. J. Pendock, A. Nirmalathas, and G. Edvell, "Transmission improvement in fiber wireless links using fiber Bragg gratings," *IEEE Photon. Technol. Lett.*, vol. 17, no. 1, pp. 190–192, Jan. 2005.

[7] C. Lim, M. Attygalle, A. Nirmalathas, D. Novak, and R. Waterhouse, "Analysis of optical carrier-to-sideband ratio for improving transmission performance in fiber-radio links," *IEEE Trans. Microw. Theory Tech.*, vol. 54, no. 5, pp. 2181–2187, May 2006.

[8] H. Toda, T. Yamashita, T. Kuri, and K. Kitayama, "25-GHz channel spacing DWDM multiplexing using an arrayed waveguide grating for 60-GHz band radio-on-fiber systems," in *Proc. IEEE MWP*, Budapest, Hungary, 2003, pp. 287–290.

[9] D. Guckenberger, "Microwave photonic applications for silicon photonics," in *Proc. OSA/OFC/NFOEC*, Los Angeles, CA, 2009, pp. 1–3.

[10] C. K. Madsen and J. H. Zhao, *Optical Filter Design and Analysis*. Hoboken, NJ: Wiley, 1999.

[11] J. F. Bauters, M. J. R. Heck, D. John, D. Dai, M.-C. Tien, J. S. Barton, A. Leinse, R. G. Heideman, D. J. Blumenthal, and J. E. Bowers, "Ultra-low-loss high-aspect-ratio Si$_3$N$_4$ waveguides," *Opt. Exp.*, vol. 19, no. 4, pp. 3163–3174, Feb. 2011.

[12] L. Zhuang, D. Marpaung, M. Burla, W. Beeker, A. Leinse, and C. Roeloffzen, "Low-loss, high-index-contrast Si$_3$N$_4$/SiO$_2$ optical waveguides for optical delay lines in microwave photonics signal processing," *Opt. Exp.*, vol. 19, no. 4, pp. 23 162–23 170, Nov. 2011.

[13] C. R. Doerr, L. Chen, Y.-K. Chen, and L. L. Buhl, "Wide bandwidth silicon nitride grating coupler," *IEEE Photon. Technol. Lett.*, vol. 22, no. 19, pp. 1461–1463, Oct. 2010.

[14] F. Morichetti, A. Canciamilla, M. Martinelli, A. Samarelli, R. M. De La Rue, M. Sorel, and A. Melloni, "Coherent backscattering in optical microring resonators," *Appl. Phys. Lett.*, vol. 96, no. 8, pp. 081112-1–081112-8, Feb. 2010.

[15] F. Morichetti, A. Canciamilla, and A. Melloni, "Statistics of backscattering in optical waveguides," *Opt. Lett.*, vol. 35, no. 11, pp. 1777–1779, Jun. 2010.

[16] R. Hernandez, A. Loayssa, and D. Benito, "On the use of single-sideband modulation for optical vector network analysis," in *Proc. IEEE MWP*, Budapest, Hungary, 2003, pp. 173–176.

[17] S. Iezekiel, "Measurement of microwave behavior of optical links," *IEEE Microw. Mag.*, vol. 9, no. 3, pp. 100–120, Jun. 2008.